ELSEVIER

Journal of Chromatography A, 779 (1997) 73–89

JOURNAL OF CHROMATOGRAPHY A

In situ analysis of protein chromatography and column efficiency using magnetic resonance imaging

Nia S. Mitchell[a], Lars Hagel[b], Erik J. Fernandez[a,*]

[a]*Department of Chemical Engineering, Thornton Hall, University of Virginia, Charlottesville, VA 22903, USA*
[b]*Research and Development, Pharmacia Biotech AB, S 751-82 Uppsala, Sweden*

Received 26 November 1996; received in revised form 1 April 1997; accepted 21 April 1997

Abstract

Magnetic resonance imaging has been used to visualize size-based protein separations inside operating chromatography columns. The effects of flow nonuniformity have been observed and analyzed quantitatively through concentration profiles of tracers measured inside the column. Analysis of these profiles provides local and averaged intracolumn plate height values for characterization of dispersion and flow nonuniformity. The magnetic resonance measurements compare favorably with conventional chromatographic measurements of column efficiency and provide more detailed insights into nonideal column performance. © 1997 Elsevier Science B.V.

Keywords: Magnetic resonance imaging; Column efficiency; Proteins

1. Introduction

While the design of chromatography columns and development of packing procedures has led to significant improvements in analytical and preparative chromatographic performance, much of this development work has been performed empirically and largely with only the chromatogram at the outlet as a measure of efficiency. This alone supplies little specific information to guide improvements in such design. In addition, for large diameter columns with compressible or unstable (e.g., silica) media, evolution of the column packing can contribute to flow nonuniformity and limit the life of a column. With the increased use of preparative chromatography in commercial practice, development of column designs and packing procedures offer opportunities to improve process efficiency. Experimental techniques which provide insights into solute peak dispersion and flow profiles throughout the distribution system and column bed are desirable to improve the rational evaluation and development of new column designs and packing techniques.

Direct measurements of flow and transport in chromatography columns have been hindered by the opaque nature of most porous media. Dye–tracer visualization has been used, however this is often limited to the column exterior [1] or to destructive evaluation of the column packing [2]. Electrochemical methods have been used to study dispersion in columns, although these studies have provided information about flow uniformity at a limited number of locations in small diameter columns [3–5]. With this approach, useful information has been provided about the effects of column walls on packing [6]. Recently, fluorescence techniques have been applied

*Corresponding author.

PII S0021-9673(97)00457-3

to investigate macroscopic flow distribution in analytical HPLC columns [5].

In parallel with its rapid development for clinical diagnosis over the last two decades, magnetic resonance imaging (MRI) has been exploited as a tool for analysis of flow and transport in porous media. Beginning with model porous media and petroleum reservoir rock [7,8], magnetic resonance methods have found broad application in the study of flow and transport in porous media and other complex, multiphase systems [9–11]. Over the past few years, MRI has been effective in evaluating elution of single components [12–14] and separations of small molecules [15]. Such studies have provided information about flow nonuniformity [12,16], flow instability [13,14], intraparticle diffusion [17] and dispersion [18]. These magnetic resonance studies of chromatography have the distinct advantage that they can be performed on intact columns during normal operation.

To date, the MRI visualization studies of chromatography have been largely qualitative and limited to small, specialized MR-visible contrast agents. And while MR signal profiles can be converted to concentration profiles with proper calibration procedures, such quantitative analysis has been applied only to cross-sectionally averaged one-dimensional profiles [19] and two-dimensional slices [20]. In this study we have extended these MRI techniques to visualize the chromatographic separation of proteins. In addition, to provide quantitative analysis of column efficiency, careful calibration procedures are performed to obtain true three-dimensional concentration distributions during a single solute elution. This information is used to characterize local and global flow inhomogeneities and sample dispersion inside an operating column.

2. Methods

2.1. Chromatography

For size exclusion chromatography (SEC), a 30×1 cm column was used (Superdex 200 10/30, Pharmacia Biotech, Piscataway, NJ, USA). The average particle diameter for this media is 13 μm. The fractionation range (M_r) for globular proteins is 10 000 to 600 000. Experiments were also performed in smaller 1 ml columns (3 cm×6.4 mm) packed with 15 μm diameter cation exchange media (SOURCE 15Q, Pharmacia Biotech, Uppsala, Sweden). The columns were characterized chromatographically at Pharmacia (Uppsala, Sweden) by running 1 μl acetone in an ethanol–water mixture (50% v/v) through the column at a flow-rate of 1 ml/min. The peak was detected at 280 nm, and plate number and asymmetry factor were calculated. For MRI experiments on the SEC column performed at the University of Virginia, all samples (0.1 ml volume) were eluted with 0.01 *M* phosphate buffer containing 0.15 *M* NaCl, at 1 ml/h. For the cation exchange columns, 0.6 *M* NaCl was used to prevent binding of the gadolinium ion tracer (Magnevist, Berlex Laboratories, Wayne, NJ, USA) by the stationary phase. For all experiments, the column was mounted horizontally in the magnet. Samples were loaded using an injection loop and valve (Model #5020, Rheodyne, Cotati, CA, USA).

2.2. MRI

Magnetic resonance imaging was performed at 1.75 Tesla using a FLASH technique [21] based on three-dimensional phase encoding. The gradient echo time was 4.9 ms, the repetition time was 22.0 ms and the tip angle used was approximately 40°. A gradient pulse at the end of the pulse sequence was used to spoil residual transverse magnetization. 128 points were collected in the readout direction along the length of the column and 32×64 phase encoding steps were used in the transverse directions. Two signal averages yielded a total acquisition time of 90 s. The imaging field-of-view for the SEC experiments was 9 cm along the axis of the column and 1.5 cm in the transverse directions, leading to a spatial resolution of 0.23×0.47×0.7 mm. For the smaller columns, the field-of-view was reduced to increase the spatial resolution to 0.2×0.4×0.35 mm. The images were collected approximately every two minutes as the sample was eluted. The degree of "blurring" in the images is less than the distance travelled in the full image acquisition time because most of the image signal intensity is collected during a short period in the middle of the acquisition time. Birdcage resonators [22] were used for signal de-

tection (3.2 cm I.D.×10 cm length for the 10 mm diameter columns and 1.7 cm I.D.×5 cm length for the 6 mm I.D. columns). Quantitative analysis of the MRI data was performed with IDL (Research Systems Inc., Boulder, CO, USA).

2.3. Protein labelling

Bovine serum albumin (BSA; A-6918, Sigma, St. Louis, MO, USA) and chymotrypsinogen A (CTA; C-4879, Sigma) were used without further purification and labelled with gadolinium diethylenetriaminepentaacetic acid (Gd-DTPA) anhydride (D-6148, Sigma), largely in accordance with the procedure of Ogan et al. [23]. Because the anhydride reagent is bifunctional, the concentration of protein was reduced to minimize the degree of protein crosslinking. Briefly, 0.256 g of either protein was dissolved in 100 ml of 0.1 *M* HEPES buffer, pH 8.9. Gd-DTPA anhydride (200 moles:mole protein) was dissolved in 2 ml DMSO and added to the dissolved protein at room temperature in several small aliquots; the pH was adjusted to 8.5 after each addition. The mixture was allowed to react while stirred for 90 min. Unbound Gd-DTPA anhydride was removed in three rounds of ultrafiltration (10 000 or 30 000 MWCO membrane, Amicon, Beverly, MA, USA) carried out at 4°C in which the protein solution was diluted to 350 ml of citrate buffer (0.1 *M*, pH 6.5) and concentrated to approximately 50 ml. $GdCl_3 \cdot 6H_2O$ (27,852-1, Aldrich, Milwaukee, WI, USA) dissolved in 1 ml of H_2O was added (20 moles Gd/mole protein) to the protein solution in five aliquots. Binding was allowed to proceed for at least 48 h and excess Gd was removed by exhaustive ultrafiltration as described above.

3. Results

3.1. Monitoring a desalting separation with MRI

Using MRI, the desalting of bovine serum albumin (BSA) was visualized in the Superdex size exclusion column. To allow MR-detection of the protein, it was chemically labelled with a gadolinium chelate, Gd-DTPA, which reduces the relaxation time of surrounding water molecules. The same gadolinium chelate was included in the sample as an MR-visible salt. Thus, both solutes were visualized indirectly via their influence on the strong water MR signal. Three-dimensional MR images were collected periodically during the elution of the mixed sample.

Fig. 1 shows representative two dimensional slices taken from the MRI data sets during the desalting separation. These slices were taken along the axis of the column near the beginning of the elution. Because the MRI signal is derived from water, a background signal, shown in gray, is visible outlining the column. The inlet is on the left and flow is to the right. The first several centimeters of the column are shown, and the remainder of the column extends beyond the end of the RF coil. Strong contrast between the labelled proteins and the solvent water has been achieved by using a large excitation tip angle and a repetition time (22 ms) much less than the T_1 of buffer without solute. The short water T_1 in the vicinity of the solutes allows much greater signal recovery compared to buffer alone. While the sample band is largely uniform over the cross-section, a region of slower flow at the column axis is evident. Both sides of the sample band show similar nonuniformity, indicating contributions from the distributor or packing are responsible as opposed to mild viscous fingering [13]. A number of runs were performed on the column, and Fig. 1 may indicate the early stages of fouling in the packing or the inlet frit.

Fig. 2 is a three-dimensional rendition of the solute band from the same datasets presented in Fig. 1. Fig. 2a shows the sample near the inlet soon after injection. Despite the broad fractionation range and intermediate molecular mass of BSA (66 000), the separation proceeds readily. A short time later some resolution of the two bands is already visible (see arrows in Fig. 2b). By Fig. 2c the two bands are completely resolved. While there is some flow nonuniformity evident (see arrows in Fig. 2a), the separation of the salt is not strongly compromised. In our experience with several different types of SEC columns, most of the flow nonuniformities seem induced by the distribution and regions of packing near the inlet given normal packing procedures ([20] and other data not shown). These effects appear to be minimal here. In this case, the separation within the column is mainly limited by the sample size used.

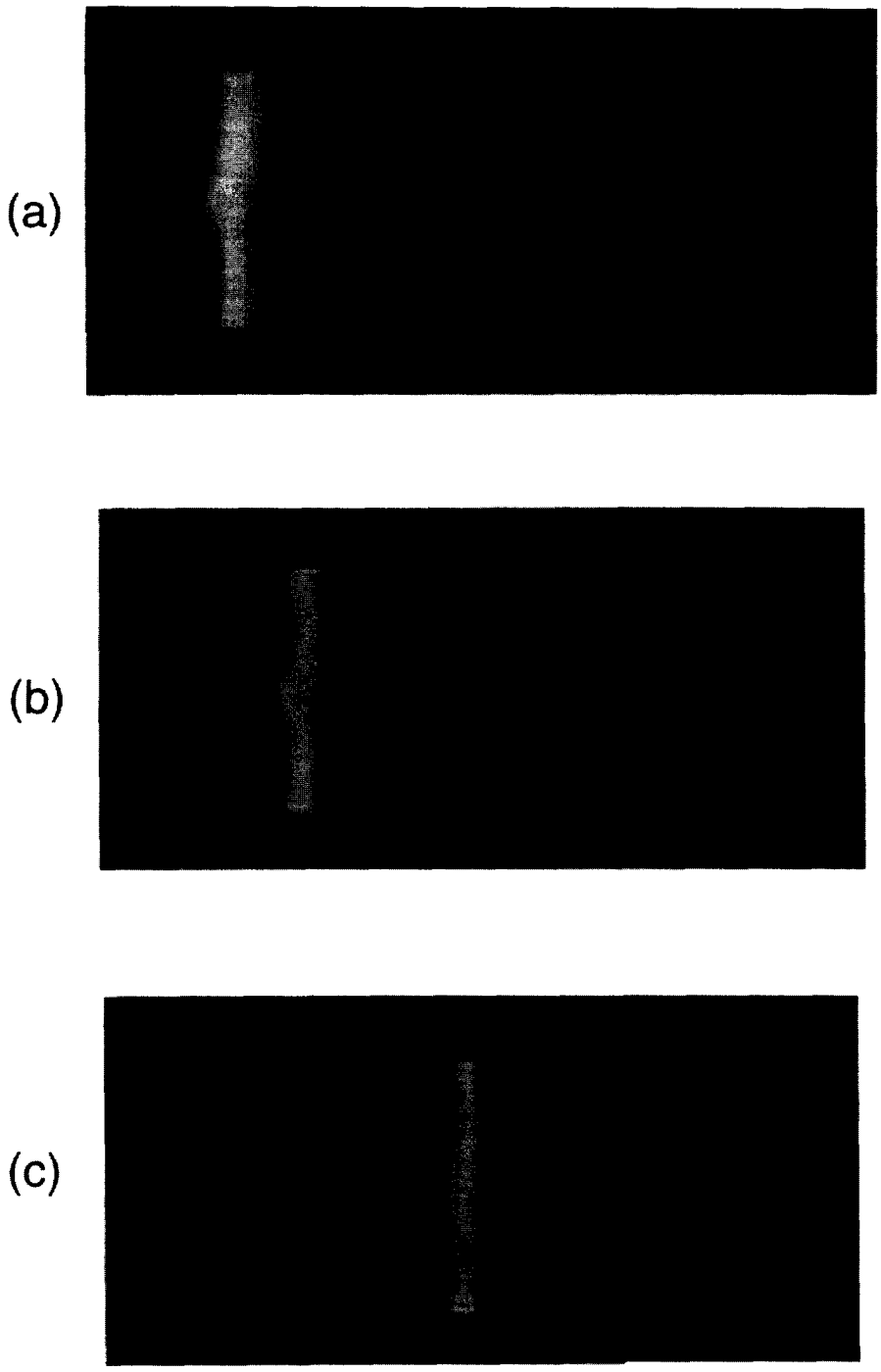

Fig. 1. Two-dimensional slices from 3D MRI images of desalting on the Superdex column. Slices were taken along the axis of the column. Column inlet is to the left and flow is to the right. Time between (a) and (b) was approximately 5 min; time between (b) and (c) approximate 10 min. The flow-rate was 5 ml/h. The field of view of the image is 9 cm horizontally and 1.5 cm vertically.

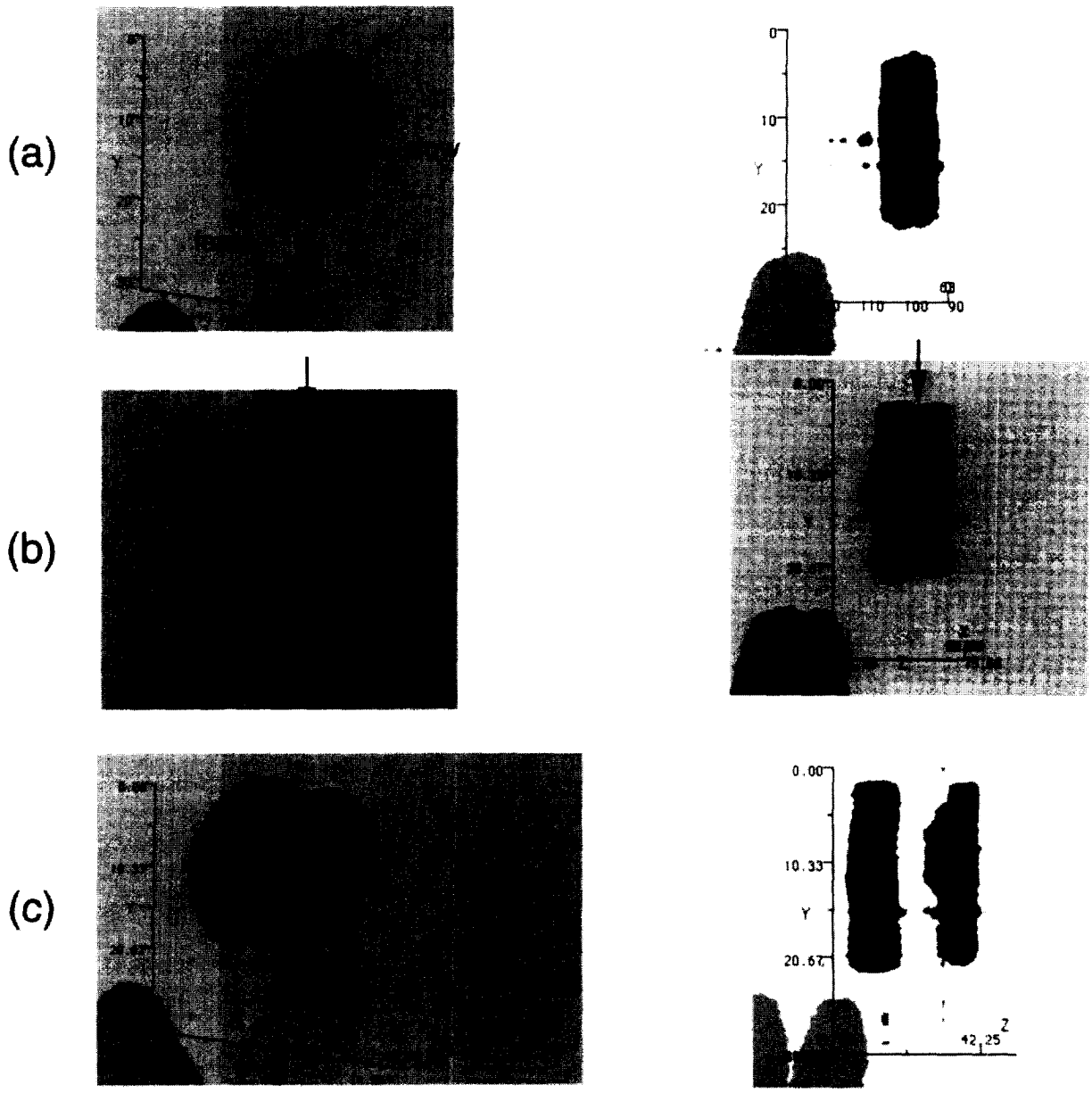

Fig. 2. Three-dimensional MRI of desalting. Views from the end of the column (angled views, left column) and side (right column) were constructed from the same MRI datasets as used in Fig. 1a–c. The surface shown is one of constant MR signal intensity. The distances on axes are expressed in image pixel number.

3.2. Size-based protein separation

MRI was also used to monitor the separation of two proteins on the Superdex column. In this case, BSA and chymotrypsinogen A (CTA) were both labelled with the gadolinium chelate, making them visible during a size-based separation. For this more difficult separation, a larger portion of the column was required to accomplish separation than in the desalting case. Therefore, to allow MRI visualization

of the entire process, the column was moved during the elution process to keep the mixed sample within the NMR detection coil.

Fig. 3 shows three dimensional MR images of the migration of the mixed sample on the SEC column. MRI is sensitive enough to document the entire course of the separation. Selected images show the loading of the sample (Fig. 3a), early resolution of a second band (Fig. 3b) and almost complete resolution of two bands (Fig. 3c). The appearance of an unexpected third band was noted in two-dimensional MRI (data not shown) which turned out to be composed of impurities from both protein samples. Size exclusion chromatograms of both proteins revealed impurities at higher molecular masses. Samples of the labelled proteins yielded nearly identical chromatograms to the unlabelled proteins, indicating that the impurities were present in the raw protein rather than being created by the labelling process. The fact that the impurities appear on the MRI indicates they were also labelled with Gd-DTPA and were most likely proteins, e.g., BSA dimers.

3.3. Concentration profiles within a column

The above experiments exemplify how MRI can reveal flow nonuniformities through measurements of sample displacements as a function of time. For quantitative analysis, it would be useful to relate these signal intensity profiles to solute concentration distributions. This is possible for a single solute given the known effect of the relaxation label, Gd-DTPA, on the NMR signal.

For the FLASH MR imaging experiment with RF spoiling between scans as used here, the signal intensity is given by

$$S = k\rho\exp(-T_G/T_2)\sin\alpha\frac{1-\exp(-T_R/T_1)}{1-(\cos\alpha)\exp(-T_R/T_1)} \quad (1)$$

where an RF pulse with tip angle α is used to observe nuclei with spin–lattice relaxation time T_1 and spin–spin relaxation time T_2 [24]. The constant k is determined by experimental apparatus and conditions, ρ is the local concentration of nuclei, T_R is the repetition time, and T_G is the experimental gradient echo time. In our case, the repetition time is short, but comparable to the T_1 range produced by the contrast agent. The relaxation times are dependent on the concentration of the relaxation agent (protein or Gd-DTPA alone). A commonly used relation for the concentration dependence is [25]

$$\frac{1}{T_1} = \frac{1}{T_{1,0}} + R_1 c \quad (2)$$

where $T_{1,0}$ is the relaxation time of water in the porous medium in the absence of the relaxation agent, c is the concentration of the relaxation agent, and R_1 is a constant ("relaxivity") which is a property of the relaxation agent. In the ion exchange columns, the relaxation time of water was determined to be 0.75 s by a standard inversion recovery method. A form similar to Eq. (2) is commonly observed for T_2 relaxation as well. For Gd-DTPA enhanced relaxation, the parameters for T_1 and T_2 relaxation are similar [26]. Using these forms in Eq. (1) gives the plot in Fig. 4 for the parameters of our experiment. At low concentrations, the rise in signal intensity is caused by enhanced recovery of signal between scans arising from increased T_1 relaxation. At higher concentrations the signal intensity declines due to enhanced T_2 relaxation during the gradient echo time (T_G). It is evident that at very low concentrations of contrast agent, the signal intensity is strongly dependent on concentration.

To achieve a monotonic and sensitive relationship between signal intensity and concentration, we performed the quantitative experiments at Gd-DTPA concentrations below 0.0025 *M*. Over this concentration range, calibrated signal intensities were measured by loading large (0.5–1.0 ml) volumes of sample onto the 1 ml ion exchange columns and collecting three-dimensional FLASH MR images under the same conditions to be used for the subsequent flow visualization experiments. A small tube containing 0.0025 *M* Magnevist without chromatographic particles was also included as an intensity reference to account for any changes in machine settings, coil tuning, machine instabilities, etc. Average signal intensities were then measured over the region of the reference tube and the region of the column occupied by the sample. Fig. 5 shows the relationship between signal intensity and concentration obtained for the calibration samples. At

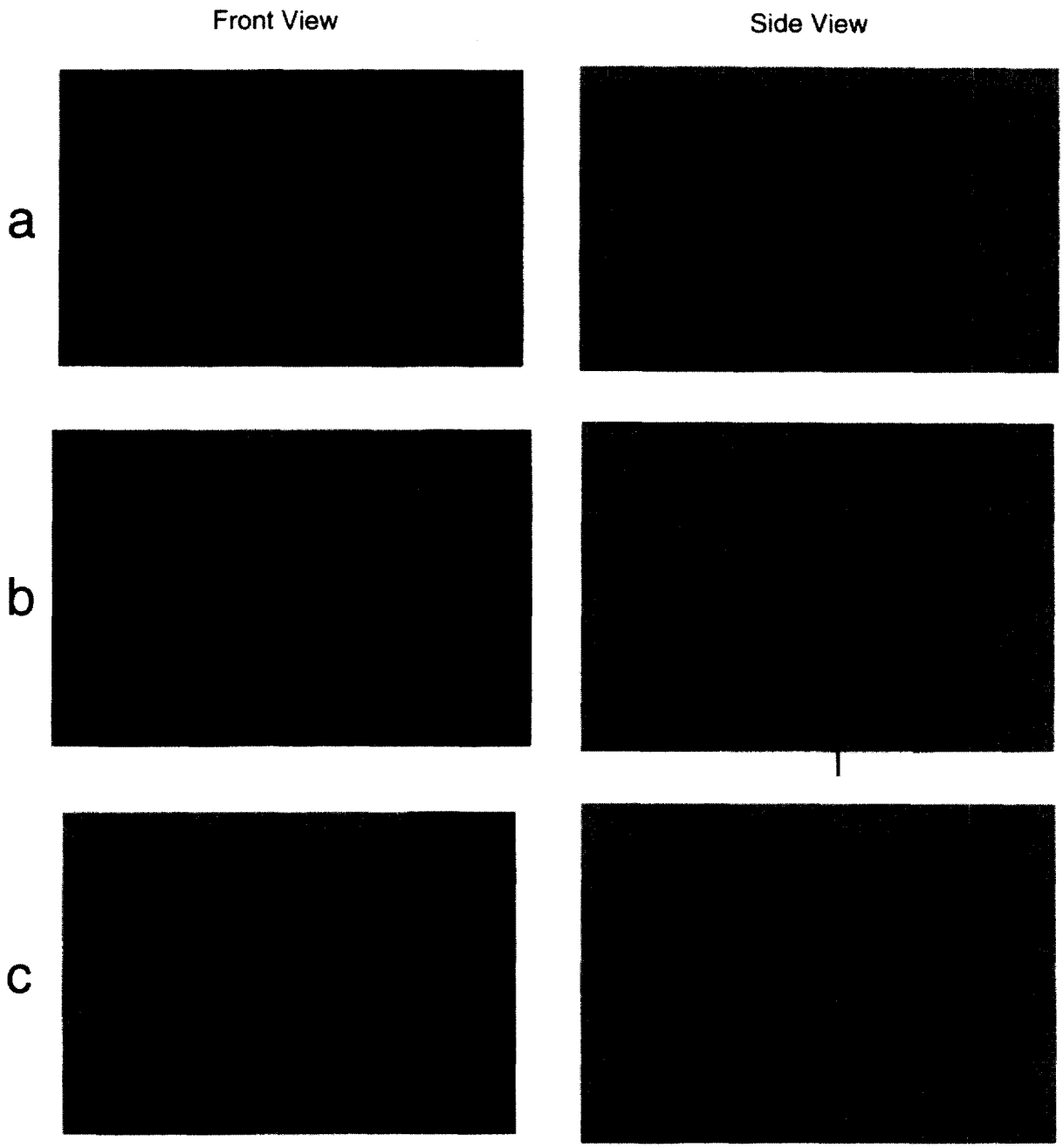

Fig. 3. Three-dimensional MRI of protein separation. Three dimensional views from the end and side of the column are shown. Time between (a) and (b) is approximately 28 min; time between (b) and (c) is approximately 15 min. Flow is from left to right. The distances on axes are expressed in image pixel number.

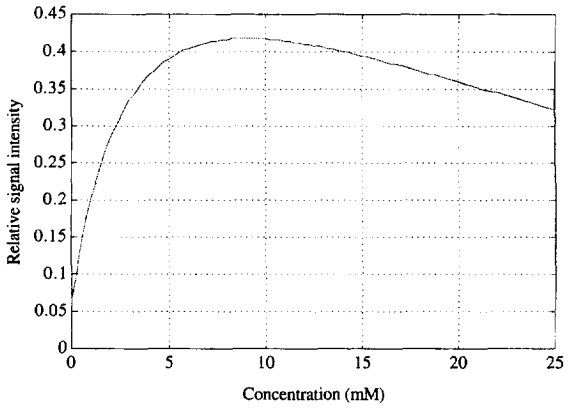

Fig. 4. Relative signal intensity as a function of Gd-DTPA concentration in the column. $T_{1,0}$ was measured to be 0.5 s. A relaxivity of 3.8 (s $mM)^{-1}$ for free Gd-DTPA at 75 MHz was obtained from [25]. T_R=20.2 ms, T_G=6.4 ms, tip angle=40°.

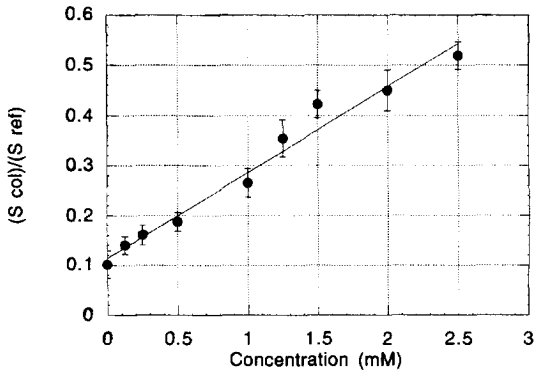

Fig. 5. Signal intensity in ion-exchange column relative to the signal intensity in the reference tube containing 0.0025 *M* Gd-DTPA. Error bars represent the measured standard deviation in signal intensity relative to the reference.

the relatively low concentrations of Gd-DTPA used here, signal intensity is roughly linearly related to solute concentration. At 0.0025 *M* Gd-DTPA, the MR signal intensity in the column is approximately a factor of 5 higher than for buffer alone; this is in good agreement with the calculations presented in Fig. 4. Therefore, as a working calibration curve, a weighted linear regression was used as shown in Fig. 5.

3.4. Intracolumn variance and HETP

As a test of this calibration method and a general test of MRI sensitivity to packing heterogeneities, five of the small ion exchange columns were packed with different types of anomalies. As described in the methods, acetone chromatograms were collected from each of the columns while in a vertical position. Plate heights (HETP) and asymmetry factors obtained chromatographically along with a brief description of the packing anomaly for each column are given in Table 1. HETP values were determined from the peak width measured at half height. In addition to the peak variance, the asymmetry factor, A_s, was calculated to characterize the tailing of the peaks. The asymmetry factor is defined as the distance from the center of the peak to the trailing edge of the peak relative to the distance from the center of the peak to the leading edge of the peak. These distances were measured at 10% of the peak height, and the center of the peak was taken to be the peak maximum. Table 1 shows that columns 4 and 5 exhibited the greatest loss of chromatographic efficiency consistent with the severe packing anomalies imposed. It is interesting to note that for these types of packing conditions the chromatographic efficiency was strongly correlated with the degree of peak asymmetry.

For each column, a series of approximately 20 three-dimensional MR images was collected during the elution of a small volume sample of Gd-DTPA.

Table 1
Chromatographic measures of column efficiency

Column	HETP (μm)	A_s	Packing description
1	135	2.4	Low pressure
2	117	2.1	Low pressure
3	97	1.7	High pressure
4	370	4.4	High pressure, 2 mm gel removed from top of bed
5	15 000	5.7	High pressure, column not filled with gel

A mobile phase linear velocity of 1.4 mm/min, corresponding to a reduced velocity of approximately 0.7, was used for all experiments.

The calibration results described above were then used to determine the three-dimensional concentration distributions within the columns for each image. One-dimensional solute profiles at each time point were determined by averaging the solute concentration over the column cross-section. These "intracolumn chromatograms" were analyzed to determine peak variance, σ^2, from peak width at half height. Because moment-based calculations of peak variance are sensitive to baseline errors, peak widths were used for variance and HETP calculations except where noted below. The analysis was repeated to obtain a "local" variance based on an axial concentration profile obtained by averaging over only a small, user-specified region of the column cross-section. This sub-region constituted a small percentage (<10%) of the column cross-section. To minimize the effects of baseline errors on peak width and variance calculations, a small baseline correction was performed using the values of the concentration profile in the column on both sides of the solute peak. Examples of the axial concentration profiles from column 1 are shown in Fig. 6. Profiles were obtained by calculating at each axial position an average concentration over the entire (Fig. 6a) or a small portion (<10%) (Fig. 6b) of the column cross-section. For this particular image and profile, the sample is near the inlet of the column. Differences between the symmetry and breadth of the profiles between local and cross-sectionally averaged profiles such as those in Fig. 6 indicate the presence of flow nonuniformities which contribute dramatically to both band asymmetry and loss of chromatographic resolution.

The calculation of the local and cross-sectionally averaged peak variance was carried out for all five columns. A plot of the two variances as a function of sample position on column 1 is shown in Fig. 7a. Variances were only calculated for MR images in which the solute band was completely on the col-

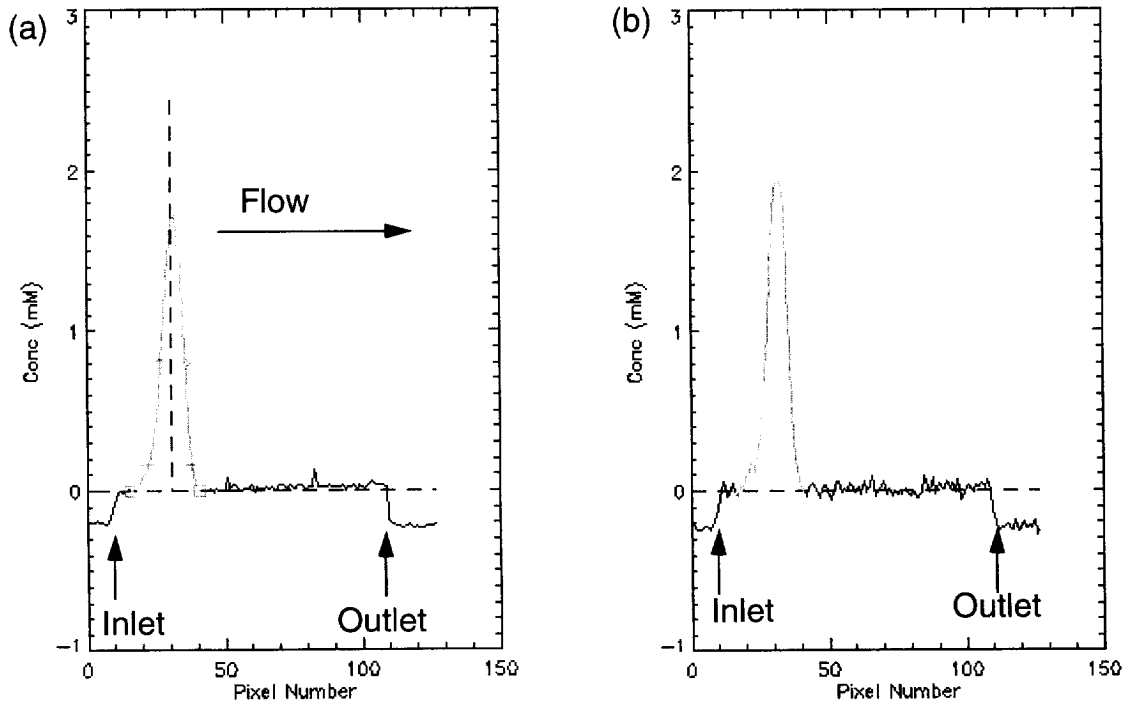

Fig. 6. Example concentration profiles taken from column 1. Left: Cross-sectionally averaged profile. Right: Locally averaged profile. The shaded portion of the profiles is the region used to calculate peak variances. The symbols on the cross-sectionally averaged peak indicate the half-height points, 10% points and baseline points used for calculations. The regions of negative concentration represent regions outside the column where the MR calibration curve is not valid.

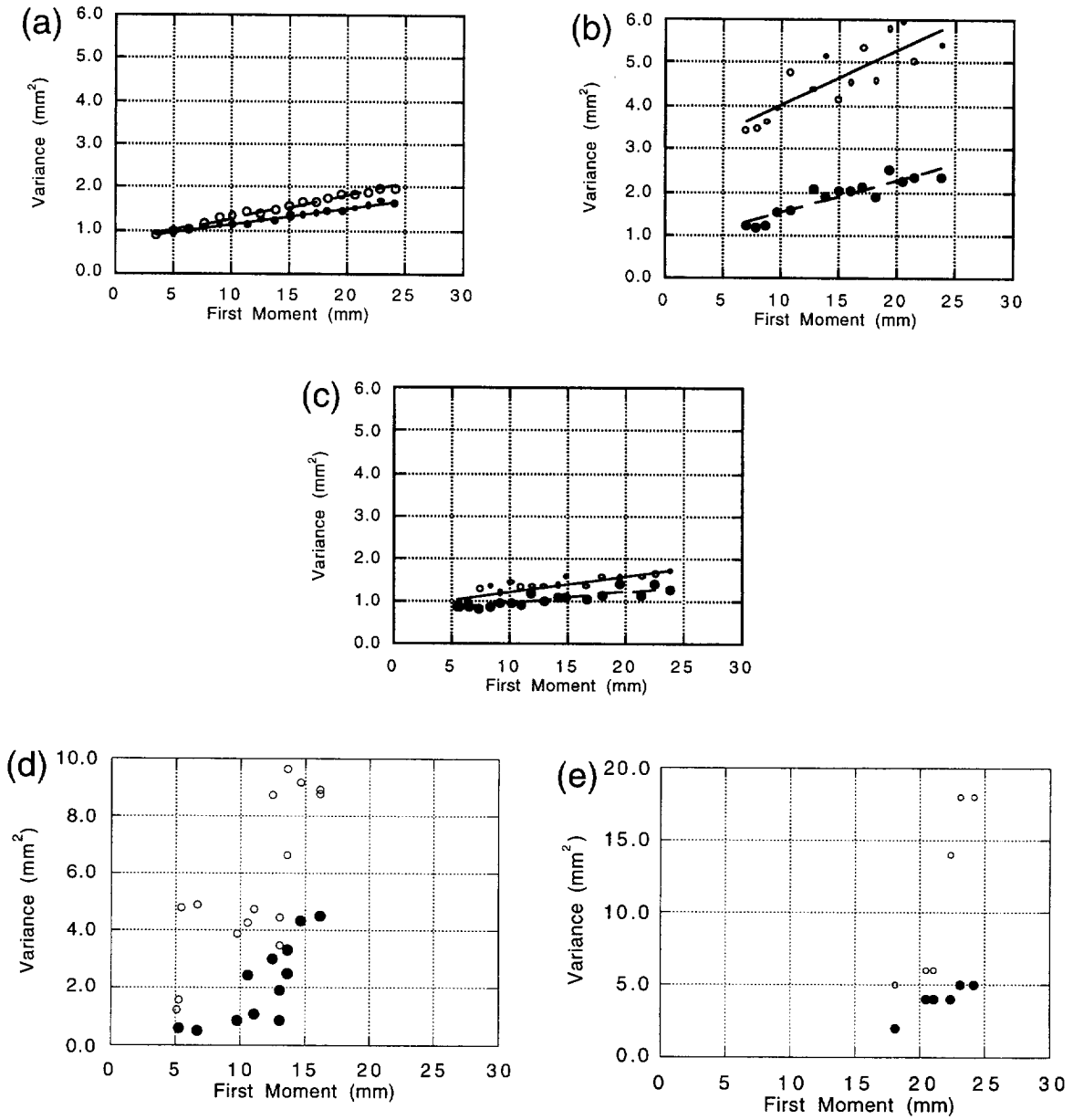

Fig. 7. Peak variance vs. column position determined by MRI. Locally averaged (closed circles) and cross-sectionally averaged profiles (open circles) were used to calculate variance as described in the text. For columns 1–3 (a–c), linear regression fits to the data are shown.

umn. Consequently, there are gaps in the variance data near the column inlet and outlet. Fig. 7 demonstrates that the variance increases with distance travelled as expected. For all five columns, the variances of the globally averaged profiles are larger than those of corresponding locally averaged profiles. This indicates that sample position must be nonuniform over the column cross-section. Indeed, a review of slices from the 3D MR images of the sample elution (see Fig. 8) confirms this to be the case. For columns 1–3, MRI shows that while the sample distribution or packing near the inlet was

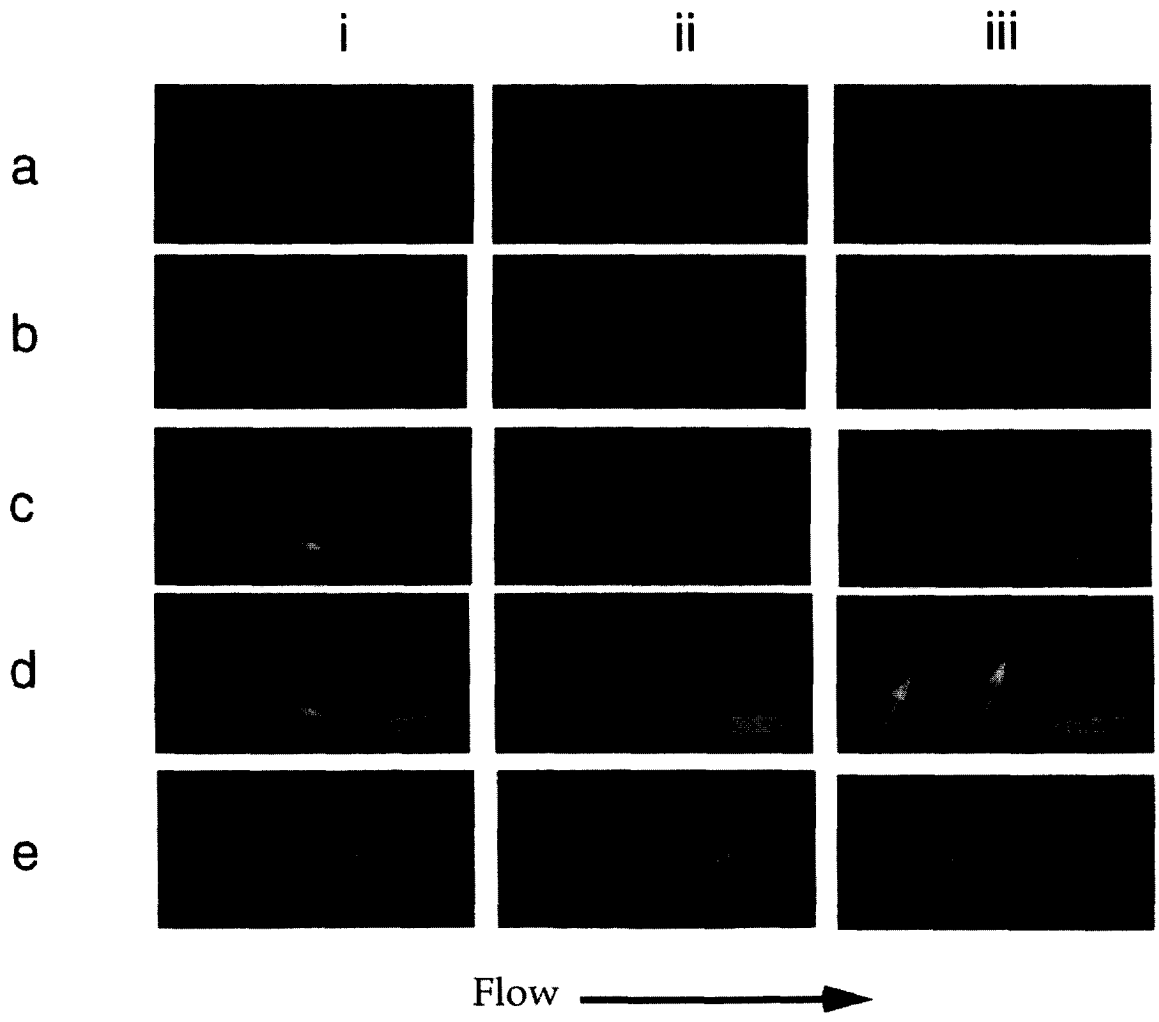

Fig. 8. Two-dimensional slices taken from three-dimension MR images of sample elution on ion-exchange columns. A set of three images collected from each column is shown in each row. Flow-rate, 1 ml/h, left to right. Sample volume, 20 μl; 2.5 m*M* Magnevist. Images shown were obtained 15 min apart except for column 5 where severe channelling occurred and images shown were collected approx. 5 min apart. In columns 3 and 4 the signal reference tube is indicated by an arrow (image 3.i, 4.i). In column 4 (image 4.iii) two air pockets are indicated.

nonuniform (see Fig. 8ai,bi,ci), the sample band profiles changed less in the body of the column (see images i–iii of Fig. 8a–c). This indicates that poor packing and/or sample distribution near the inlet were dominant contributors to flow nonuniformity in these columns.

These results can be expressed more quantitatively in terms of height equivalent to a theoretical plate (HETP). The plate height can be obtained from the plots of the variance through [27]

$$\mathrm{HETP} = \frac{\partial(\sigma)^2}{\partial z} \tag{3}$$

where σ^2 is the peak variance and z is the position of the peak on the column. For a homogeneously packed column without extracolumn band broadening, the plot of variance vs. axial position should be a straight line with zero intercept. Indeed, for the first three columns (Fig. 7a–c) the plots of the locally and globally determined variance are nearly straight

lines. The globally averaged variance is higher but shows a similar slope. A linear least squares curve fit of the variance data gives the lines shown in Fig. 7. Plate heights were calculated from the MR data in two ways: (1) by dividing the variance obtained from the last concentration profile by the length of column travelled, and (2), according to Eq. (3), using linear curve fits of the data in Fig. 7a–c. For each method, plate heights were calculated based on both cross-sectional and local profiles. The intercept of the linear curve fit was used to estimate the initial variance at the column inlet.

The cross-sectionally averaged plate heights determined by MRI are roughly comparable to those determined by chromatography listed in Table 1. Both techniques confirm that the first three columns are much more efficient than columns 4 and 5. Both measures identify column 3 as having the highest efficiency. The plate heights determined by MRI are generally somewhat lower than those measured by chromatography except for column 2. Indeed, the MRI measurements of variance should be lower than those obtained by chromatography since the effects of nonuniform column packing and extracolumn effects at the end of the column are not being measured.

The HETP values determined from local profiles are consistently smaller than those based on cross-sectionally averaged profiles, indicating that the contributions of flow nonuniformity to band broadening are significant. For the columns with the least serious flow nonuniformities (columns 1–3), the local HETP values based on Eq. (3) give reduced HETP values of approximately 2, indicating that the dispersion in the smaller regions chosen is close to that of an ideally packed column. Given the slow flow-rate used here (reduced velocity of ~0.7), molecular diffusion effects likely contributed to the dispersion. Thus, the HETP might have been even lower if a flow-rate at the minimum of the van Deemter curve had been employed. For columns 4 and 5, both the local and cross-sectionally averaged HETP values are substantially higher. The MR images in Fig. 8d–e reveal that strong nonuniform flow occurred throughout the length of these two beds. In these two cases the velocity gradients were so large that even when a small fraction (~10%) of the cross-section was used to calculate a "local" profile, flow variations still contributed strongly to the variance.

The variance measured near the inlet of the columns can reveal the extent to which extracolumn effects, flow distribution and the packing at the inlet of the column deteriorate performance. It can be seen in Fig. 7 that column 2 exhibited a much larger cross-sectionally averaged variance near the inlet than did columns 1 or 3. This indicates that flow distribution and/or nonuniform packing near the inlet and not just sample volume contributed significantly to initial band broadening for this column. Columns 1 and 3 exhibit lower local and averaged variances at the inlet, but they are still nonzero. The two-dimensional MR images of Fig. 8 reveal some of the nature of the flow nonuniformity for columns 1–3. While the patterns vary, much of the distortion in the sample band is already evident in the first image of the sample near the inlet, while smaller changes in the sample band shape occur later in the column. The MR images of Fig. 8a–c clearly show that flow nonuniformity due to nonideal distribution and/or nonuniform packing near the inlet are also significant for columns 1 and 3.

As is apparent in Fig. 7a, the first variance measurement for column 1, taken approximately 2 mm from the inlet, was already 0.8 mm^2. Extrapolating to the inlet, the global and local variance were estimated to be approximately 0.8 mm^2 (see Table 2). Of this initial sample band broadening, the contribution of finite sample size to the variance is expected to be equal to approximately $L^2_{sample}/5$, where L_{sample} is the length of the square sample in the column [28,29]. For the 20 μl sample volume used, this contribution to variance should be roughly 0.24 mm^2. Although the MRI estimate of variance assumes a gaussian shape while the sample volume contribution to broadening will be different, it appears that there may be an additional variance contribution measured by MRI. Such additional peak broadening could be caused by nonuniform flow inside: (1) the few fittings and short (few cm) tubing connecting the injection valve to the column, (2) the spaces in the column header/distributor, and/or (3) the distributing frit at the top of the bed. The differences between the MRI-determined global and local variances indicate the degree to which flow variations over the cross-section of the distributor,

Table 2
MR measurements of column efficiency

Column	HETP (μm)				Estimated initial variance[c] (mm^2)		A_s^d
	Based on final profile[a]		Eq. (3)[b]				
	Average	Local	Average	Local	Average	Local	
1	82	67	52	36	0.8	0.8	1.3
2	230	100	128	73	2.7	0.8	2.7
3	71	54	35	26	0.9	0.7	1.4
4	540	250	–	–	–	–	~2.0
5	740	210	–	–	–	–	>2

[a] An HETP averaged over the column length determined from peak width measurements obtained from the final MR concentration profiles.
[b] HETP determined by Eq. (3). The slope was determined from linear regression of all the variance values for each of the local or cross-sectionally averaged sets of variance in Fig. 7a–c.
[c] The variance at the inlet was extrapolated as the intercept of the best fit regression line for the variance vs. column length data in Fig. 7a–c.
[d] The asymmetry factor was calculated based on the last cross-sectionally averaged MR profile obtained for each column.
MR measurements of plate heights were obtained from peak widths measured at half-height (final concentration profile) and slopes of the variance curves in Fig. 7. Both cross-sectional averaged profiles ("Average") and local profiles were used to calculate HETP. Initial variances were not calculated for columns 4 and 5 because they could not be accurately extrapolated. The A_s value could not be determined accurately for column 4 because of the disturbances in the MR images.

frit and early part of the bed contribute to band broadening. While the cross-sectionally averaged variances estimated at the inlet are larger than the local ones (see Table 2), they are close in size, suggesting that extracolumn dispersion due to sample volume and nonuniform flow in the external fittings is important. However, further analysis is necessary to determine the size, significance and location of each of the sources of band broadening.

Column 4 exhibited a different kind of macroscopic flow nonuniformity. In this case, the column was packed at high pressure, leaving a 2 mm gap between the bed and the top frit. In shipment and in the course of experimentation, the packing apparently redistributed to yield two large air bubbles a few mm across as shown in Fig. 8d. The air bubbles acted as obstructions, producing very nonuniform flow which gave broad peaks by chromatography (see Table 1 and Fig. 9d). The MR measurements of variance shown in Fig. 7d are also quite high compared to the previous columns. The quantitative analysis of the MR data was complicated by the fact that the air bubbles gave no MR signal, and thus did not fall on the MR calibration curve. Thus, the column 4 variance measurements shown in Fig. 7d must be considered qualitative. As expected, the profiles do show much higher variance values and slope of the variance curve consistent with the very nonuniform flow throughout the column. Even with the problems associated with the obstructions, the MR data give variances which do correlate approximately with the chromatography data (compare HETP values in Table 2 with Table 1).

The fifth column examined showed severe peak broadening due to poor packing method used. Here again, the column was not completely filled with chromatographic media, but was filled with buffer after being partially packed at high pressure. When the column was placed on its side for MRI analysis, the media appeared to settle, leaving a gap at the top of the column which allowed for severe channelling. This channelling is evident in Fig. 8e, which shows MR images indicating sample preferentially travelling quickly along the top edge of the column. Accordingly, this column yielded extremely poor chromatographic resolution and strong asymmetry (see Table 1 and Table 2 and the chromatograms of Fig. 9e). The rapid flow of parts of the sample through the column limited the number of data points obtained for Fig. 7. In this case, it is likely that the packing rearranged significantly, and thus, the specific flow patterns leading to peak tailing in chromatograms and MR concentration profiles were probably different. Nonetheless, the quantitative MR data analysis shows rapidly increasing variance through the column and poor HETP values consistent with the conventional chromatography data. The MR-derived A_s value is lower, but the MR baseline

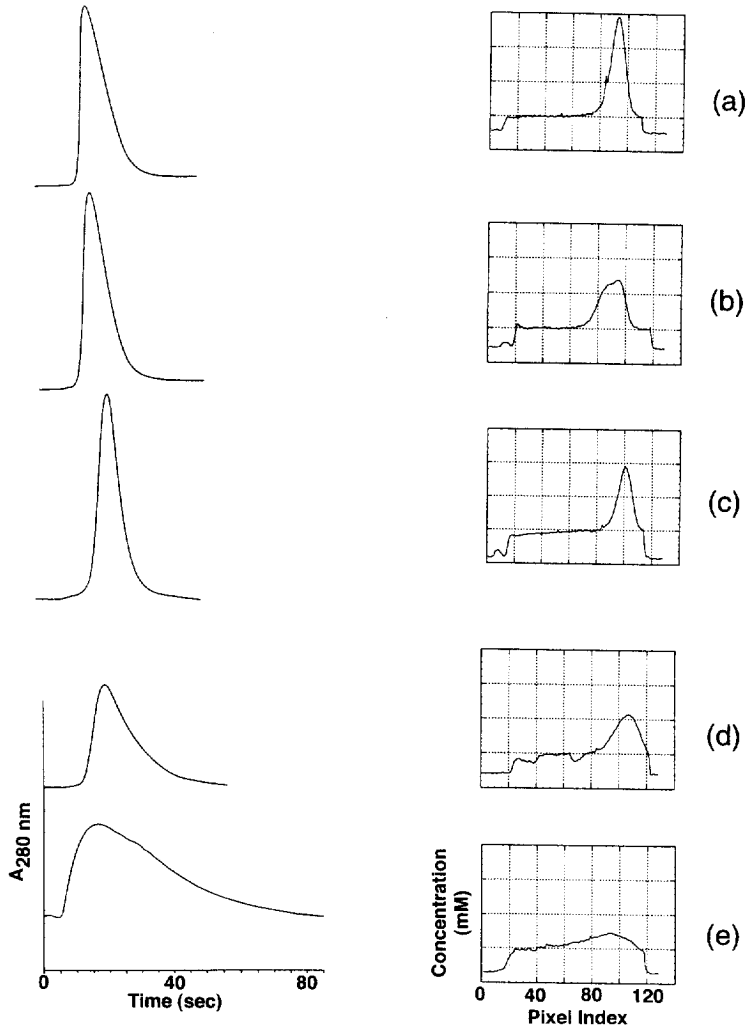

Fig. 9. Chromatograms and MRI-derived concentration profiles obtained from ion-exchange columns.

is somewhat ambiguous and the profile used probably does not have all the sample tails on the column (see MR concentration profile in Fig. 9e).

Fig. 9 presents a comparison of conventional chromatograms with concentration profiles obtained by MRI near the outlet of each column. The tailing patterns vary somewhat between the columns, due to the different flow patterns present in each column. The MR-derived concentration profiles for columns 1 and 3 look at least qualitatively similar to the chromatographic results. Column 2 shows a more complex and broad concentration profile within the column (Fig. 9b) and a higher HETP value (Compare Table 2 and Table 1) than obtained by chromatography. Even if the MR-determined concentration profile shown in Fig. 9b was not broadened any further in the remainder of the column or the outlet, the average HETP would still be greater than that observed chromatographically. Thus, it appears that the packing prepared under low pressure for this column (see Table 1) may have shifted in transit between the chromatographic measurements performed at Pharmacia in Sweden and the MR measurements performed at the University of Virginia. This may be a tangible demonstration of the instability of columns packed at low pressure.

4. Discussion

In this work, magnetic resonance imaging visualization has been used to visualize protein desalting and protein–protein separation operations within an operating column. In this preliminary study, the effect of column packing and distribution nonuniformity on the quality of the separation could be assessed throughout the column with three-dimensional MRI. In the prepacked column, flow nonuniformities were found to be small but measurable. Direct measurements by MRI should prove useful for further detailed assessment of column design, packing procedures and packing evolution on separation quality. In addition, the ability to visualize solutes during a developing separation could prove useful for the study of nonlinear chromatography, although the effects of strong adsorption on the relaxation properties of MR labels used here would have to be considered carefully. It should be noted that the MR visualization approach used here is based on the water signal, allowing only one component to be identified individually at one time. However, repeating the chromatographic elution with a different component labelled each time could provide information about multiple components. In addition, MR spectroscopic imaging approaches have recently been applied to visualize multicomponent chromatographic separations [30].

The MR images shown in Fig. 8 show flow patterns somewhat similar to those observed in previous MR studies of chromatography columns [15,16]. It is interesting to note that these flow nonuniformities are not necessarily radially symmetric and lead to considerable peak asymmetry (tailing) in the resulting chromatograms. Also, the HETP estimates obtained here by MRI are considerably less (especially locally) than estimates obtained chromatographically. This is in accord with previous, less carefully calibrated estimates of HETP by MRI [15]. Finally, consistent with earlier MRI studies of chromatography columns [13,15,20], many of the packing nonuniformities appear to be concentrated near the column inlet. This suggests that the initial and final aspects of the packing procedure and the boundaries of the column may have a great impact on the resultant column packing. While this and other previous MRI studies are providing a view of flow nonuniformities in columns, further detailed study is required to determine the precise relationship between packing procedures and column design and the resulting packing nonuniformities.

The detailed analysis of MR images of tracer elution under nonadsorbing conditions carried out here has shown that straightforward FLASH MRI imaging approaches can quantitatively assess peak broadening and flow nonuniformity. In the test performed here, the peak variance measurement provided a useful measure of the dispersion which is consistent with chromatographic measures in these columns. The 3D FLASH MRI measurements allow assessment of dispersion values throughout almost the entire bed. The locally measured values are in line with other measurements of column efficiency in well packed columns [3,4,18]. Measurements of local and averaged variance near the inlet revealed that extracolumn effects and/or dispersion in the flow distribution system were important in the small ion exchange columns. The disparity between local and averaged variances near the inlet revealed the importance of nonuniform sample application, showing that this approach may be useful for characterizing flow distribution separately and, in addition, to flow uniformity within the bed.

This approach complements other tools which have been developed to characterize dispersion and flow in chromatography columns. For example, elegant microelectrode and optical sensor techniques have provided accurate and sensitive information about dispersion and flow uniformity, although at a limited number of locations within the bed and with the requirement of electrode implantation within the column [3–5]. While the MR methods do require that column materials of construction be nonmetallic, or at least non-ferromagnetic, the column can be analyzed intact. For the measurement of dispersion, pulsed-field-gradient (PFG) NMR methods have been recently applied to chromatography columns [18], although the results have been limited to averaged measurements over large portions of a column to date. However, the ability to combine NMR imaging with PFG measurements [10] means that local measurements should be close at hand. One potential advantage of the approach described here, however, is that the local dispersion measurements can be made directly on the solute of interest

with the high sensitivity of the water signal. Direct PFG measurements of solute dispersion might be precluded due to sensitivity considerations.

There are certainly limitations to the quantitative analysis method described here. While the entire bed can be visualized by MRI, the quantitative analysis presented here utilizes the full sample, which precluded calculations from the initial few millimetres of the column, given the sample broadening induced by extracolumn effects and the distribution system. Improved injection procedures should help in this regard. Also, while the MR data averaged over the full cross-section provided high quality concentration profiles, the local measurements were less precise. Signal- and contrast-to-noise of the MR concentration profiles may be further improved through further optimization of the relaxation agent concentration relative to the MR experimental sequence parameters. It should be noted that image signal-to-noise was sacrificed for spatial and temporal resolution in this study. The signal-to-noise of the measurements could be increased measurably through use of a coarser spatial resolution or stopping the elution at a small number of time points to allow signal averaging.

In summary, this approach provides a complementary perspective on dispersion and nonuniform flow in columns. Together with MR visualization, the variance analysis will provide quantitative and much more detailed information about column efficiency than traditional chromatographic methods and could prove helpful in the development and evaluation of future column designs and operating procedures. Indeed, MRI visualization has recently guided the development of a column design to reduce the deleterious effects of viscous fingering [31].

Acknowledgments

The authors would like to thank Karl-Gunnar Hellström and Torvald Andersson for preparing the ion exchange columns and providing the chromatography measurements. We would also like to thank Matt Dickson for helpful discussions and assistance with MR experiments and Tucker Norton for assistance in data analysis. Robert G. Bryant also provided helpful insights into water relaxation. Helpful comments on the manuscript from Eric Grund are gratefully appreciated.

Financial support for this work has been provided by the National Science Foundation (BCS 9210199) and Pharmacia Biotech AB.

References

[1] J.C. Janson, J. Agric. Food Chem. 19 (1971) 581.
[2] S. Yamamoto, M. Nomura, Y. Sano, J. Chem. Eng. Jpn. 19 (1986) 227.
[3] J.H. Knox, G.R. Laird, P.A. Raven, J. Chromatogr. 122 (1976) 129.
[4] C. Eon, J. Chromatogr. 149 (1978) 29.
[5] T. Farkas, J.Q. Chambers, G. Guiochon, J. Chromatogr. A 679 (1994) 231.
[6] J.H. Knox, J.F. Parcher, Anal. Chem. 41 (1969) 1599.
[7] R.J. Gummerson, C. Hall, W.D. Hoff, R. Hawkes, G.N. Holland, W.S. Moore, Nature 281 (1979) 56.
[8] H.J. Vinegar, J. Pet. Tech. 38 (1986) 257.
[9] A. Caprihan, E. Fukushima, Phys. Rep. 198 (1990) 195.
[10] P.T. Callaghan, Principles of Nuclear Magnetic Resonance Microscopy, Oxford University Press, New York, 1991.
[11] L.F. Gladden, Chem. Eng. Sci. 49 (1994) 3339.
[12] E. Bayer, W. Müller, M. Ilg, K. Albert, Angew. Chem. Int. Ed. Engl. 28 (1989) 1029.
[13] L.D. Plante, P.R. Romano, E.J. Fernandez, Chem. Eng. Sci. 49 (1994) 2229.
[14] E.N. Lightfoot, A.M. Athalye, J.L. Coffman, D.K. Roper, T.W. Root, J. Chromatogr. A 707 (1995) 45.
[15] U. Tallarek, E. Baumeister, K. Albert, E. Bayer, G. Guiochon, J. Chromatogr. A 696 (1995) 1.
[16] E. Bayer, E. Baumeister, U. Tallarek, K. Albert, G. Guiochon, J. Chromatogr. A 704 (1995) 37.
[17] S.J. Gibbs, E.N. Lightfoot, T.W. Root, J. Phys. Chem. 96 (1992) 7458.
[18] E. Baumeister, U. Klose, K. Albert, E. Bayer, G. Guiochon, J. Chromatogr. A 694 (1995) 321.
[19] G. Guillot, G. Kassab, J.P. Hulin, P. Rigord, J. Phys. D: Appl. Phys. 24 (1991) 763.
[20] E.J. Fernandez, C.A. Grotegut, G.W. Braun, K.J. Kirschner, J.R. Staudaher, M.L. Dickson, V.L. Fernandez, Phys. Fluids A 7 (1995) 468.
[21] A. Haase, J. Frahm, D. Matthaei, K.D. Merboldt, W. Hänicke, J. Magn. Reson. 67 (1986) 217.
[22] C.E. Hayes, W.A. Edelstein, J. Magn. Reson. 63 (1985) 622.
[23] M.D. Ogan, U. Schmiedl, M.E. Moseley, W. Grodd, H. Paajanen, R.C. Brasch, Invest. Radiol. 22 (1987) 665.
[24] A. Haase, Magn. Reson. Med. 13 (1990) 77.
[25] T. Andersson, L. Hagel, Anal. Biochem. 141 (1984) 461.
[26] J.C. Sternberg, in: J.C. Giddings, R.A. Keller (Eds.), Advances in Chromatography, Vol. 2, Marcel Dekker, New York, 1966.

[27] J.C. Giddings, Dynamics of Chromatography, Marcel Dekker Inc., New York, 1965.
[28] R.W. Stout, J.J. DeStefano, L.R. Snyder, J. Chromatogr. 261 (1983) 189.
[29] L. Hagel, J. Chromatogr. 324 (1985) 422.
[30] M.L. Dickson, T.T. Norton, E.J. Fernandez, AIChE J., (1996) in press.
[31] E.J. Fernandez, T.T. Norton, W.C. Jung, J.S. Tsavalas, Biotechnol. Prog. 12 (1996) 480.